

# Modular network for high-rate quantum conferencing

Carlo Ottaviani,<sup>1,\*</sup> Cosmo Lupo,<sup>2</sup> Riccardo Laurenza,<sup>3</sup> and Stefano Pirandola<sup>1,4,†</sup>

<sup>1</sup>*Computer Science and York Centre for Quantum Technologies, University of York, York YO10 5GH, UK*

<sup>2</sup>*Department of Physics and Astronomy, University of Sheffield, Hounsfield Road, Sheffield, S3 7RH, UK*

<sup>3</sup>*QSTAR, INO-CNR and LENS, Largo Enrico Fermi 2, 50125 Firenze, Italy*

<sup>4</sup>*Research Laboratory of Electronics, Massachusetts Institute of Technology, Cambridge, Massachusetts 02139, USA*

One of the main open problems in quantum communication is the design of efficient quantum-secured networks. This is a challenging goal, because it requires protocols that guarantee both unconditional security and high communication rates, while increasing the number of users. In this scenario, continuous-variable systems provide an ideal platform where high rates can be achieved by using off-the-shelf optical components. At the same time, the measurement-device independent architecture is also appealing for its feature of removing a substantial portion of practical weaknesses. Driven by these ideas, here we introduce a modular design of continuous-variable network where each individual module is a measurement-device-independent star network. In each module, the users send modulated coherent states to an untrusted relay, creating multipartite secret correlations via a generalized Bell detection. Using one-time pad between different modules, the network users may share a quantum-secure conference key over arbitrary distances at constant rate.

PACS numbers: 03.65.Ud, 03.67.-a, 42.50.-p

Quantum communication [1–3] with continuous variables (CV) systems [4–6] has attracted increasing attention over the past years. In particular, quantum key distribution (QKD) has been a rapidly developing field [7]. Theoretical studies have considered one-way protocols with coherent states [8–10], thermal protocols [11–16], and two-way protocols [17–21], with a number of experimental demonstrations [22–32]. It is known that CV-QKD protocols may achieve very high rates. As a matter of fact, ideal coherent-state protocols [9] may achieve rates as high as half of the Pirandola-Laurenza-Ottaviani-Banchi bound [33, 34] for private communication over a lossy channel, i.e.,  $-\log_2(1 - \eta)$  bits per use, with  $\eta$  being the channel transmissivity (see Ref. [35] for a recent review on bounds for private communication).

In addition to point-to-point protocols, there has been effort towards network implementations [36–38]. An important step is the design of a scalable QKD network whose rate is high enough to compete with the classical infrastructure. Another feature to achieve is an end-to-end architecture where middle nodes may be untrusted. The first steps in this direction were moved in 2012 with the introduction of a swapping protocol based on an untrusted relay [39, 40], a technique that became known as “measurement-device independence” (MDI), and recently extended to CV-QKD [41–46]. However, until today, MDI protocols have been limited to a small number of remote users, e.g., 2 in Refs. [39], or 3 in Ref. [47].

In this work we remove these limitations. In particular, we introduce a modular architecture that combines trusted and untrusted nodes, as well as quantum and classical communication methods, allowing secure quan-

tum conferencing among an arbitrary number of users. At the core of our design there are MDI star-network modules, interconnected by shared nodes, which can run one-time pad protocols between different modules. Each module consists of a central (untrusted) relay performing a general N-mode Bell detection that allows an arbitrary number of users to share the same quantum conference key. The security of the protocol is first proven in the asymptotic limit of many signals exchanged, and then extended to the composable setting which incorporates finite-size effects. This modular design is scalable, because it allows us to increase arbitrarily the number of users and the achievable distance between them, while maintaining a high and constant rate. Moreover, it can be implemented using linear optical elements, and it allows to add extra modules resorting just on classical communication protocols. From this point of view the scheme is very flexible and represents a good prototype to be developed into a large scale CV-QKD network.

## I. RESULTS

### A. Modular network for quantum conferencing

In our modular architecture, each individual module is a star network running a multipartite MDI-QKD quantum conferencing protocol based on the generalization of symmetric CV-MDI-QKD [43]. Each star-network module  $M_i$  is labeled by  $i = 1, \dots, N^*$  and host  $N_i$  users. The generic user  $k$  in module  $M_i$  sends bright coherent states [4]  $|\alpha_k^i\rangle$  to a central untrusted relay, whose amplitude  $\alpha_k^i$  is Gaussianly modulated with variance  $\mu_k^i$ . With no loss of generality we may assume that  $\mu_k^i$  is the same for any  $k$ , so that we may associate a single variance parameter  $\mu_i$  to module  $M_i$ . The eavesdropping is assumed to be performed by entangling cloners [7], so that the link

\*Electronic address: carlo.ottaviani@york.ac.uk

†Electronic address: stefano.pirandola@york.ac.uk

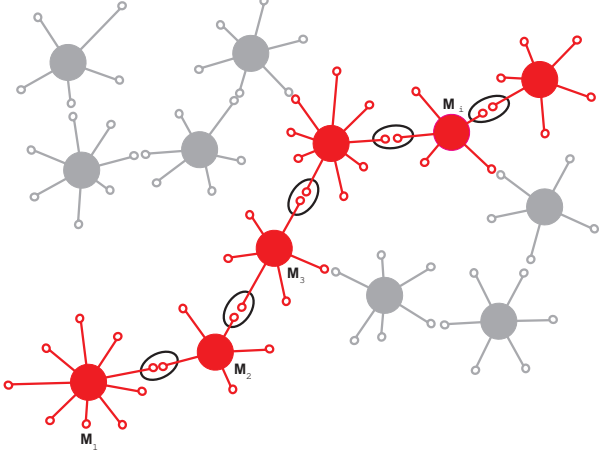


FIG. 1: Modular network for secure quantum conferencing. Each module  $M_i$  is a continuous-variable (CV) measurement-device-independent (MDI) quantum key-distribution (QKD) star network, composed by a central untrusted relay and  $N_i$  trusted users, whose connections are independently affected by loss and noise. Each module  $M_i$  first runs an independent protocol of quantum conference key-agreement. Because two different modules have a shared trusted user, we may implement classical one-time pad sessions where the keys from each module are processed into a final common key for the entire network.

connecting the arbitrary user  $k$  to the relay in module  $M_i$  is described by two parameters: the transmissivity  $\eta_k^i$  of the link, and its thermal noise  $\bar{n}_k^i$ .

Within module  $M_i$  the untrusted relay performs a multipartite Bell detection on the incoming  $N_i$  modes; this consists of a suitable cascade of beam-splitters followed by  $N_i$  homodyne detections, as shown in Fig. 2. The homodynes on the left measure quadratures  $\hat{q}_2, \dots, \hat{q}_{N_i}$ , while the single one on the right measures  $\hat{p}$ . The outcomes of the measurements are combined into the global outcome  $\gamma_i := (q_2, \dots, q_{N_i}, p)$ . After  $\gamma_i$  is broadcast to the users of the module, their individual variables  $\alpha_k^i$  share correlations that can be post-processed into a secret key  $K_i$  via classical error correction and privacy amplification. All the users in module  $M_i$  reconcile their data with respect to a trusted user which is shared with another module  $M_j$ .

To reduce the parameters of the problem we may introduce the minimum transmissivity  $\eta_i = \min_{k \in [1, N_i]} \eta_k^i$  and maximum thermal noise  $\bar{n}_i = \max_{k \in [1, N_i]} \bar{n}_k^i$  associated to module  $M_i$ . From a physical point of view this is a symmetrization of the star network to the worst-case scenario, assuming all its links to have the worst combination of parameters. This condition clearly provides a lower bound  $K(\mu_i, N_i, \eta_i, \bar{n}_i)$  to the actual key rate  $K_i$  of the module. By optimizing over the Gaussian modulation, we may consider the value  $K(N_i, \eta_i, \bar{n}_i) := \max_{\mu_i} K(\mu_i, N_i, \eta_i, \bar{n}_i)$ . Once each module has generated its key, the shared nodes run sessions of one-time pad where the keys from different modules are composed to

generate a common key for all the network, with rate

$$K_{\text{net}} = \min_{i \in [1, N^*]} K(N_i, \eta_i, \bar{n}_i). \quad (1)$$

Therefore, the entire network can work at the rate of the least performing module. However, if this rate is high then the lego-like structure of the network allows all the users to communicate at the same high rate no matter how far they are from each other (see Fig. 1).

## B. Detailed description the MDI star-network module

In this section we describe the modus operandi of a single module. To simplify the notation we omit the label  $i$ . In a single module, we consider an arbitrary number  $N$  of users (or “Bobs”) sending Gaussian-modulated coherent states  $|\alpha_k\rangle$  to a middle untrusted relay, as depicted in Fig. 2. Each of the coherent states is affected by a thermal-loss channel  $\mathcal{E}$  modeled as a beam-splitter with transmissivity  $\eta$  and thermal noise  $\bar{n}$ , i.e., mixing the incoming signal with an environmental thermal state with  $\bar{n}$  mean photons. As explained before, we assume the worst-case scenario, so that  $\eta$  is the minimum transmissivity of the links and  $\bar{n}$  is the maximum thermal noise. After the action of the channel  $\mathcal{E}$  on each link, the states are detected by a multipartite  $N$ -mode Bell detection.

This detection consists of a suitable cascade of beam-splitters followed by  $N$  homodyne detections. More precisely, we have a sequence of beam-splitters with increasing transmissivities  $T_k = 1 - k^{-1}$  for  $k = 2, \dots, N$  as depicted in Fig. 2. Then, all the homodynes at the left measure the  $\hat{q}$ -quadrature while the final one at the bottom measures the  $\hat{p}$ -quadrature, with global outcome  $\gamma := (q_2, \dots, q_N, p)$  (see Supplementary Notes 1 and 2 for further description). One can check that this measurement ideally projects onto a displaced version of an asymptotic bosonic state  $\Psi$  that realizes the multipartite Einstein-Podolsky-Rosen (EPR) conditions  $\sum_{k=1}^N \hat{p}_k = 0$  and  $\hat{q}_k - \hat{q}_{k'} = 0$  for any  $k, k' = 1, \dots, N$ .

After the classical outcome  $\gamma$  is broadcast to the users, their individual variables  $\alpha_k$  will share correlations which can be post-processed into secret keys via error correction and privacy amplification. We may pick the shared trusted user as the one encoding the key, with all the others decoding it in direct reconciliation [7].

## C. Entanglement-based representation

Let us write the network in entanglement-based representation. For each user, the coherent state  $|\alpha\rangle$  can be generated by using a two-mode squeezed vacuum (TMSV) state  $\Phi_{AB}$  where mode  $B$  is subject to heterodyne detection. The random outcome  $\beta$  of the detection is fully equivalent to prepare a coherent state on mode  $A$  whose amplitude  $\alpha$  is one-to-one with  $\beta$  [41]. Recall

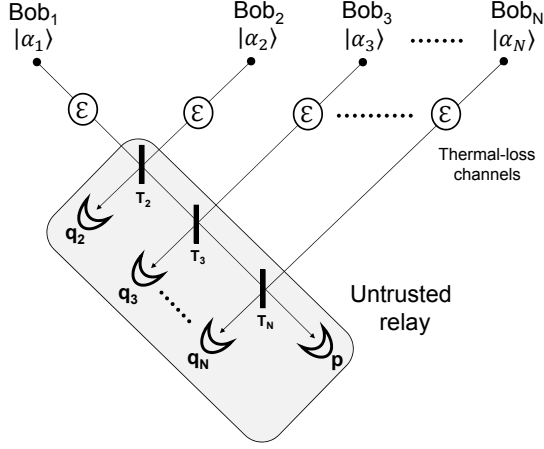


FIG. 2: Each Bob sends a Gaussian-modulated coherent state  $|\alpha_k\rangle$  to an untrusted relay through a link which is described by a thermal-loss channel  $\mathcal{E}$  with transmissivity  $\eta$  and thermal noise  $\bar{n}$ . At the relay, the incoming states are subject to a multipartite continuous-variable (CV) Bell detection, by using a cascade of beam splitters with transmissivities  $T_k = 1 - k^{-1}$  for  $k = 2, \dots, N$ , followed by homodyne detectors in the  $\hat{q}$  or  $\hat{p}$  quadrature as shown in the figure. The global outcome  $\gamma = (q_2, \dots, q_N, p)$  is broadcasted to the Bobs, so that a posteriori correlations are created in their local variables  $\alpha_1, \dots, \alpha_N$ . These correlations are used to extract a secret key for quantum conferencing.

that a TMSV state is a Gaussian state with covariance matrix (CM) [4]

$$\mathbf{V}_{AB} = \begin{pmatrix} \mu \mathbf{I} & \sqrt{\mu^2 - 1} \mathbf{Z} \\ \sqrt{\mu^2 - 1} \mathbf{Z} & \mu \mathbf{I} \end{pmatrix}, \quad \begin{cases} \mathbf{Z} := \text{diag}(1, -1), \\ \mathbf{I} := \text{diag}(1, 1), \end{cases} \quad (2)$$

where parameter  $\mu \geq 1$  quantifies the noise variance of each thermal mode. Up to factors [41], parameter  $\mu$  also provides the variance of the Gaussian modulation of the coherent amplitude  $\alpha$  on mode  $A$  after heterodyning  $B$ .

Assume that the users have  $N$  copies of the same TMSV state, whose  $A$ -part is sent to the relay through a communication channel  $\mathcal{E}$ . Also assume that the CM of the two-mode state after the channel has the form

$$\mathbf{V}'_{AB} = \begin{pmatrix} x \mathbf{I} & z \mathbf{Z} \\ z \mathbf{Z} & y \mathbf{I} \end{pmatrix}. \quad (3)$$

Because we consider a thermal-loss channel with transmissivity  $\eta$  and thermal noise  $\bar{n}$ , we have  $x = \eta\mu + (1 - \eta)(2\bar{n} + 1)$ ,  $y = \mu$ , and  $c = \sqrt{\eta}\sqrt{\mu^2 - 1}$ . Then, after the Bell measurement and the communication of the outcome  $\gamma$ , the local modes  $\mathbf{B} := B_1 \dots B_N$  are projected onto a symmetric  $N$ -mode Gaussian state with CM

$$\mathbf{V}_{\mathbf{B}|\gamma} = \begin{pmatrix} \Delta & \Gamma & \cdots & \Gamma \\ \Gamma & \Delta & \ddots & \Gamma \\ \vdots & \ddots & \ddots & \vdots \\ \Gamma & \Gamma & \cdots & \Delta \end{pmatrix}, \quad (4)$$

where we have set  $\mathbf{\Gamma} := (N^{-1}x^{-1}z^2)\mathbf{Z}$ , and

$$\Delta := \text{diag} \left( y - \frac{N-1}{N} \frac{z^2}{x}, y - \frac{1}{N} \frac{z^2}{x} \right). \quad (5)$$

Details on the the derivation of Eq. (4) are given in the Supplementary Note 2.

Note that the conditional state  $\rho_{B_i B_j|\gamma}$  between any pair of Bobs  $i$  and  $j$  is Gaussian with CM

$$\mathbf{V}_{B_i B_j|\gamma} = \begin{pmatrix} \Delta & \mathbf{\Gamma} \\ \mathbf{\Gamma} & \Delta \end{pmatrix}. \quad (6)$$

For  $N = 2$  this state describes the shared state in a standard CV-MDI-QKD protocol [41]. Assuming no thermal noise ( $\bar{n} = 0$ ), the state  $\rho_{B_i B_j|\gamma}$  is always entangled and we may compute its relative entropy of entanglement (REE)  $E_R(\rho_{B_i B_j|\gamma})$  [48–50] using the formula for the relative entropy between Gaussian states [33, 51]. This REE provides an upper bound to the rate achievable by any MDI-QKD protocol (DV or CV) based on a passive untrusted relay. For  $N > 2$ , one can check that the bipartite state  $\rho_{B_i B_j|\gamma}$  may become separable when we decrease the transmissivity  $\eta$ , while it certainly remains discordant [52–54]. In the multi-user scenario, the security between two Bobs may still hold because the purification of their state is held partially by Eve and partially by the other Bobs, which play the role of trusted noise. In trusted noise QKD we know that security does not rely on the presence of bipartite entanglement while quantum discord provides a necessary condition [55].

#### D. Key rate of a star-network module

Once  $\gamma$  is received, the  $i$ th Bob heterodynes his local mode  $B_i$  with random outcome  $\beta_i$ , which is one-to-one with an encoded amplitude  $\alpha_i$  in the prepare and measure description. In this way the local mode  $B_j$  of the  $j$ th Bob is mapped into a Gaussian state  $\rho_{\mathbf{B}_j|\gamma\beta_i}$  with CM  $\mathbf{V}_{\mathbf{B}_j|\gamma\beta_i}$  that can be computed using tools from Refs. [4, 56–58]. The subsequent heterodyne detection of mode  $B_j$  generates an outcome  $\beta_j$  which is one-to-one with an encoded  $\alpha_j$ . It is clear that the Bell detection at the relay and the local heterodyne measurements of the various Bobs all commute, so that we may change their time order in the security analysis of the protocol. Thus, we can derive the mutual information  $I(\beta_i : \beta_j)$  between the two Bobs. Similarly, we may compute the Holevo information  $\chi(\beta_i : \mathbf{E})$  between the  $i$ th Bob and an eavesdropper (Eve) performing a collective Gaussian attack [59–61] associated with the thermal-loss channels [4].

The expression  $K = I(\beta_i : \beta_j) - \chi(\beta_i : \mathbf{E})$ , which is a function of all the parameters of the protocol, provides the asymptotic rate of secret key generation between any pair of users (see Supplementary Note 3). This is a conferencing key shared among all Bobs; it can be optimized over  $\mu$ , and will depend on the number of Bobs  $N$  besides the channel parameters  $\eta$  and  $\bar{n}$ . Assuming a standard optical fiber with attenuation of 0.2dB per km, we

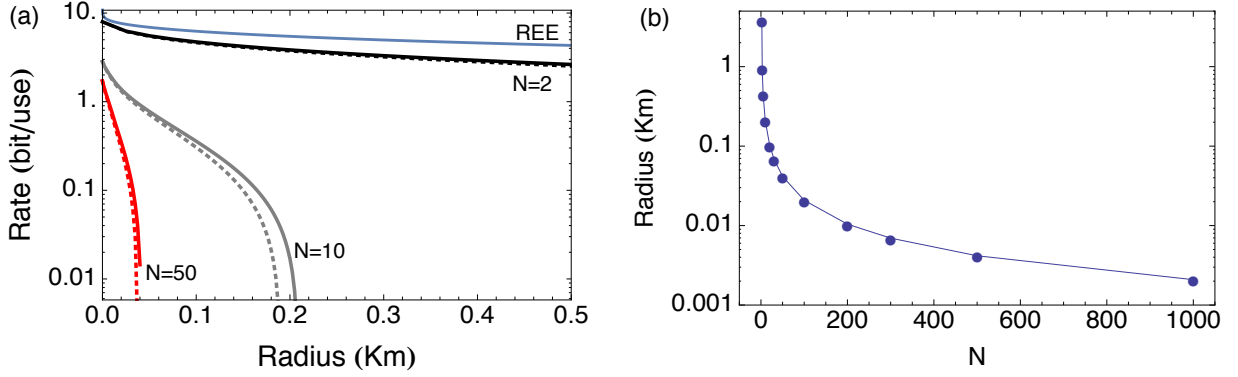


FIG. 3: Secret key rates and maximum distances for quantum conferencing. (a) We plot the conferencing key rate for a measurement-device-independent star network of  $N = 2$  (black), 10 (grey) and 50 (red) users, as a function of the fiber distance  $d$  and assuming thermal noise  $\bar{n} = 0$  (solid curves) and  $\bar{n} = 0.05$  (dashed curves). The top blue curve is the relative entropy of entanglement (REE) of the reduced bipartite state specified by Eq. (6), which upper bounds the maximal key rate achievable with standard continuous-variable measurement-device-independent quantum-key-distribution CV-MDI-QKD ( $N = 2$ ). (b) We plot the maximum fiber distance  $d$  versus the number of users  $N$  in a quantum conference.

can map the transmissivity into a fiber distance  $d$ , using  $\eta := 10^{-0.02d}$ . Therefore, we have a rate of the form  $K(\mu, N, d, \bar{n})$  which can be optimized over  $\mu$  to give the maximal conferencing rate  $K(N, d, \bar{n})$ . The maximization over  $\mu$  is required because for  $N > 2$  the maximum rate is not obtained in the limit  $\mu \gg 1$ .

The conferencing rate is plotted in Fig. 3(a) for an MDI star network with an increasing number of users  $N$ . We compare the rates over the link-distance  $d$  for different values of thermal noise  $\bar{n}$ . As expected the rate decreases for increasing  $N$ . Despite this effect, our result shows that high-rate quantum conferencing is possible. For instance, in a star network with  $N = 50$  users at about  $d \simeq 40$  m from the central relay and thermal noise  $\bar{n} = 0.05$ , the key rate is greater than  $\simeq 0.1$  bits per use. In Fig. 3(b), we set  $\bar{n} = 0$  and plot the maximum distance for quantum conferencing versus the number of users, solving the equation  $K(N, d, 0) = 0$ . We see a trade-off between maximum distance and number of users. Despite this trade-off, we conclude that fiber-optic secure quantum conferencing between tens of users (belonging to a single star-network module) is indeed feasible within the typical perimeter of a large building.

### E. Finite-size composable security

Within a module, consider a pair of Bobs,  $i$  and  $j$ , with local variables  $\beta_i$  and  $\beta_j$  after heterodyne detection. They aim at generating a secret key by reconciling on  $\beta_i$ . The error correction routine is characterized by an error correction efficiency  $\xi \in (0, 1)$  [62, 63], a residual probability of error  $\delta_{\text{EC}}$ , and an abort probability  $1 - p > 0$ . We also remark that  $\beta_i$  must be mapped into a discrete variable  $\tilde{\beta}_i$  taking  $2^d$  values per quadrature.

Consider the mutual information  $I(\beta_i : \beta_j)$  and Eve's Holevo bound  $\chi(\beta_i : \mathbf{E})$  obtained from the reduced state

of Eq. (6). Then, we have the following estimate for the  $\delta$ -secret key rate after  $n$  uses of the module [46]

$$r_n^\delta \gtrsim \xi I(\beta_i : \beta_j) - \chi(\beta_i : \mathbf{E}) - \frac{1}{\sqrt{n}} \Delta_{\text{AEP}}(2p\delta_s/3, d), \quad (7)$$

where  $\delta = \delta_s + \delta_{\text{EC}} + \delta_{\text{PE}}$ , and  $\Delta_{\text{AEP}}(\xi, d) \leq 4(d + 1)\sqrt{\log(2/\xi^2)}$ . Here the error term  $\delta_s$  is the smoothing parameter of the smooth conditional min-entropy [46]. For the Holevo bound  $\chi(\beta_i : \mathbf{E})$  we assume the worst-case value compatible with the experimental data, up to a probability smaller than  $\delta_{\text{PE}}$ . The rate  $r_n^\delta$  is obtained conditioned that the protocol does not abort and yields a  $\delta$ -secure key against collective Gaussian attacks.

The generalization to coherent attacks is obtained, as in Ref. [46], by applying a Gaussian de Finetti reduction. We find that the asymptotic rates are approximately achieved for block sizes of  $10^6 - 10^9$  data points depending on the loss and noise in the channels. Examples for  $N = 3, 5, 10$  are described in Fig. 4.

The composable security analysis starts from a parameter estimation procedure. As mentioned above, in estimating the channel parameters, we adopt the worst-case scenario where we choose the largest possible value of the thermal noise in each channel, and the lower available transmissivity, within the confidence intervals. This procedure may not be optimal at high loss, so that our estimates for the achievable communication distances are conservative estimates. Alternative (more performing) parameter estimation procedures, as those described in Refs. [65, 66], could be adapted to our network model and further improve its performance.

## II. DISCUSSION

We have introduced a network for quantum conferencing where modules can be linked together to achieve

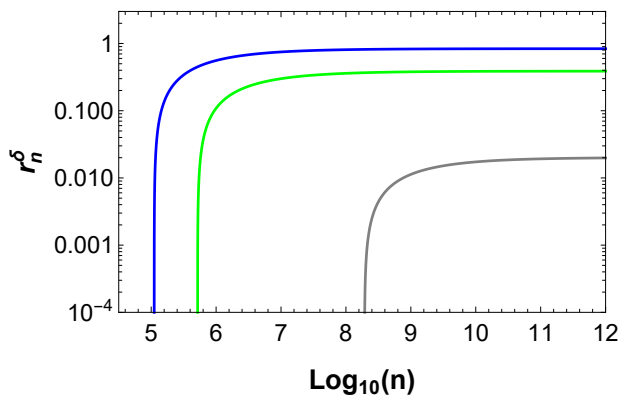


FIG. 4: Finite-size composable secret key rate  $r_n^\delta$  of Eq. (7) (bits per use) versus sample size  $n$ , for error correction efficiency  $\xi = 98\%$  [62, 63], success probability of the error correction routine  $p = 0.9$ , and security parameter  $\delta < 10^{-20}$ . The plot is obtained for a symmetric configuration with  $N$  users at a distance of 0.18km from the relay (assuming 0.2dB loss per km and thermal noise of  $\bar{n} = 0.05$  photons). From top to bottom we consider  $N = 3, 5, 10$ .

constant high-rate secure communication over arbitrarily long distances. The design of each module is based on a CV-MDI star network with many users. Our analysis shows how the secret key-rate of each star network decreases by increasing the distance from the central relay and/or the number of users. In ideal conditions, we find that 50 users may privately communicate at more than 0.1 bit per use within a radius of 40m, distance typical of a large building. With a clock of 25MHz [67], this is a key rate of the order of 2.5Mbits per second for all the users. The secret keys established in the modules are then cascaded through the entire modular network: Adjacent modules are connected by trusted users generating a common key via one-time pad sessions.

We have studied the implementation of our protocol using coherent states, which are important for practical reasons. In Supplementary Note 4, we have also considered the case where the users use squeezed states. In such a case the performance improves, both in terms of achievable distance and the number of users. In any case, we

remark that our network protocol provides a powerful application of CV-MDI-QKD that greatly outperforms its DV counterpart. In fact, while our protocol is deterministic, any linear optical implementation of a DV multi-partite Bell detection is highly probabilistic, with a probability of success scaling as  $\simeq 2^{-N}$  for  $N$  users. This means that a corresponding DV-MDI-QKD star network has an exponentially low rate no matter at what distance is implemented. See Supplementary Note 5 for details.

In Supplementary Note 6, we further analyze the performance of the protocol based on coherent states, assuming practical imperfections affecting the homodyne detectors and the beam splitters of the relay. Such undesirable features may arise from imperfect beam splitting operations, perturbing the multipartite Bell detection and degrading the performance of the scheme. Our results show that a proof-of-principle experiment is feasible with current technology, allowing to secure up to 9 users per module, over a radius of 12m.

In conclusion, let us remark that our network is based on a generalization of CV MDI-QKD, where the multiuser keys are extracted within each single module. For this reason the final key is shorter than the private key extractable by just two remote end-users. In other words, the key rate of our protocol cannot reach the existing upper bounds for end-to-end network quantum communication [68, 69] (see also Refs. [70, 71]). Finally, let us also note that additional studies may consider the multimode nature of sources and detectors, particularly for the optimized configuration of the protocol described in the Supplementary Note 4. In such a case, the security of the scheme can be recovered by applying the symmetrization of the multimode source described in Ref. [72].

## Acknowledgments

This work was supported by the EPSRC via the ‘UK Quantum Communications Hub’ (EP/M013472/1), the European Union’s Horizon 2020 research and innovation program under grant agreement No 820466 (CiViQ), and the Innovation Fund Denmark via the Quantum Innovation Center Qubiz.

- 
- [1] M. A. Nielsen, M. A. and Chuang, I. L. *Quantum computation and quantum information* (Cambridge Univ. Press, 2000).
  - [2] J. Watrous, *The theory of quantum information* (Cambridge Univ. Press, 2018).
  - [3] M. Hayashi, *Quantum Information Theory: Mathematical Foundation* (Springer, 2017).
  - [4] C. Weedbrook *et. al.* Rev. Mod. Phys. **84**, 621 (2012).
  - [5] Braunstein, S. L. & van Loock, P. Quantum information with continuous variables. *Rev. Mod. Phys.* **77**, 513-577 (2005).
  - [6] Andersen, U. L., Neergaard-Nielsen, J. S., van Loock, P.

- & Furusawa, A. Hybrid discrete- and continuous-variable quantum information. *Nat. Phys.* **11**, 713-719 (2015).
- [7] Pirandola, S., Andersen, U. L., Banchi, L., Berta, M., Bunandar, D., Colbeck, R., Englund, D., Gehring, T., Lupo, C., Ottaviani, C., Pereira, J., Razavi, M., Shaari, J. S., Tomamichel, M., Usenko, V. C., Vallone, G., Villoresi, P. & Wallden, P. Advances in Quantum Cryptography. Preprint at <https://arxiv.org/abs/1510.08863> and <https://arxiv.org/abs/1906.01645> (2019).
- [8] Grosshans, F. & Grangier, P. Continuous Variable Quantum Cryptography Using Coherent States. *Phys. Rev. Lett.* **88**, 057902 (2002).

- [9] Weedbrook, C. *et al.* Quantum cryptography without switching. *Phys. Rev. Lett.* **93**, 170504 (2004).
- [10] Ottaviani, C., Mancini, S. & Pirandola, S. Gaussian two-mode attacks in one-way quantum cryptography. *Phys. Rev. A* **95**, 052310 (2017).
- [11] Filip, R. Continuous-variable quantum key distribution with noisy coherent states. *Phys. Rev. A* **77**, 022310 (2008).
- [12] Usenko, V. C. & Filip, R. Feasibility of continuous-variable quantum key distribution with noisy coherent states. *Phys. Rev. A* **81**, 022318 (2010).
- [13] Weedbrook, C., Pirandola, S., Lloyd, S. & Ralph, T. C. Quantum Cryptography Approaching the Classical Limit. *Phys. Rev. Lett.* **105**, 110501 (2010).
- [14] Weedbrook, C., Pirandola, S. & Ralph, T. C. Continuous-variable quantum key distribution using thermal states. *Phys. Rev. A* **86**, 022318 (2012).
- [15] Weedbrook, C., Ottaviani, C. & Pirandola, S. Two-way quantum cryptography at different wavelengths. *Phys. Rev. A* **89**, 012309 (2014).
- [16] Usenko, V. C. & Filip, R. Trusted noise in continuous-variable quantum key distribution: a threat and a defense. *Entropy* **18**, 20 (2016).
- [17] Pirandola, S., Mancini, S., Lloyd, S. & Braunstein, S. L. Continuous variable quantum cryptography using two-way quantum communication. *Nat. Phys.* **4**, 726–730 (2008).
- [18] Ottaviani, C. & Pirandola, S. General immunity and superadditivity of two-way Gaussian quantum cryptography. *Sci. Rep.* **6**, 22225 (2016).
- [19] Ottaviani, C., Mancini, S., & Pirandola, S. Two-way Gaussian quantum cryptography against coherent attacks in direct reconciliation. *Phys. Rev. A* **92**, 062323 (2015).
- [20] Shapiro, J. H. Defeating passive eavesdropping with quantum illumination. *Phys. Rev. A* **80**, 022320 (2009).
- [21] Zhuang, Q., Zhang, Z., Dove, J., Wong, F. N. C. & Shapiro, J. H. Floodlight quantum key distribution: A practical route to gigabit-per-second secret-key rates. *Phys. Rev. A* **94**, 012322 (2016).
- [22] Gehring, T., Jacobsen, C. S. & Andersen, U. L. Single-quadrature continuous-Variable quantum key distribution. *Quant. Inf. Comput.* **16**, 1081–1095 (2016).
- [23] Grosshans, F. *et al.* Quantum key distribution using gaussian-modulated coherent states. *Nature* **421**, 238–241 (2003).
- [24] Madsen, L. S. *et al.* Continuous variable quantum key distribution with modulated entangled states. *Nat. Commun.* **3**, 1083 (2012).
- [25] Jouguet, P., Kunz-Jacques, S., Leverrier, A., Grangier, P., & Diamanti, E. Experimental demonstration of long-distance continuous-variable quantum key distribution. *Nat. Photon.* **7**, 378–381 (2013).
- [26] Zhang, Z. *et al.* Entanglement’s Benefit Survives an Entanglement-Breaking Channel. *Phys. Rev. Lett.* **111**, 010501 (2013).
- [27] Shapiro, J. H., Zhang, Z. & Wong, F. N. C. Secure communication via quantum illumination. *Quant. Inf. Proc.* **13**, 2171–2193 (2014).
- [28] Jacobsen, C. S., Gehring, T. & Andersen, U. L. Continuous variable quantum key distribution with a noisy laser. *Entropy* **17**, 4654–4663 (2015).
- [29] Huang, D., Huang, P., Lin, D. & Zeng, G. Long-distance continuous-variable quantum key distribution by controlling excess noise. *Sci. Rep.* **6**, 19201 (2016).
- [30] Zhang, Z., Zhuang, Q., Wong, F. N. C. & Shapiro, J. H. Floodlight quantum key distribution: Demonstrating a framework for high-rate secure communication. *Phys. Rev. A* **95**, 012332 (2017).
- [31] Zhang, Z. *et al.* Experimental quantum key distribution at 1.3 Gbit/s secret-key rate over a 10-dB-loss channel. *Quantum Sci. Technol.* **3**, 025007 (2018).
- [32] Zhang, Y.-C. *et al.* Continuous-variable QKD over 50km commercial fiber. *Quantum Sci. Technol.* **4**, 035006 (2019).
- [33] Pirandola, S., Laurenza, R., Ottaviani, C. & Banchi, L. Fundamental limits of repeaterless quantum communications. *Nat. Commun.* **8**, 15043 (2017).
- [34] Pirandola, S., Laurenza, R., Ottaviani, C. & Banchi, L. Fundamental limits of repeaterless quantum communications. Preprint at <https://arxiv.org/abs/1510.08863> and <https://arxiv.org/abs/1512.04945> (2015).
- [35] Pirandola, S. *et al.* Theory of channel simulation and bounds for private communication. *Quant. Sci. Technol.* **3**, 035009 (2018).
- [36] Kimble, H. J. The quantum internet. *Nature* **453**, 1023–1030 (2008).
- [37] Pirandola, S., Weedbrook, C., Eisert, J., Furusawa, A. & Braunstein, S. L. Advances in quantum teleportation. *Nat. Photon.* **9**, 641–652 (2015).
- [38] Pirandola, S. & Braunstein, S. L. Unite to build a quantum internet. *Nature* **532**, 169–171 (2016).
- [39] Braunstein, S. L. & Pirandola, S. Side-channel-free quantum key distribution. *Phys. Rev. Lett.* **108**, 130502 (2012).
- [40] Lo, H.-K., Curty, M., & Qi, B. Measurement-Device-Independent Quantum Key Distribution. *Phys. Rev. Lett.* **108**, 130503 (2012).
- [41] Pirandola, S. *et al.* High-rate quantum cryptography in untrusted networks. *Nat. Photon.* **9**, 397–402 (2015).
- [42] Pirandola, S. *et al.* MDI-QKD: Continuous- versus discrete-variables at metropolitan distances. *Nat. Photon.* **9**, 773–775 (2015).
- [43] Ottaviani, C., Spedalieri, G., Braunstein, S. L. & Pirandola, S. Continuous-variable quantum cryptography with an untrusted relay: Detailed security analysis of the symmetric configuration. *Phys. Rev. A* **91**, 022320 (2015).
- [44] Spedalieri, G. *et al.* Quantum cryptography with an ideal local relay. *Proc. SPIE* **9648**, 96480Z (2015).
- [45] Papanastasiou, P., Ottaviani, C. & Pirandola, S. Finite-size analysis of measurement-device-independent quantum cryptography with continuous variables. *Phys. Rev. A* **96**, 042332 (2017).
- [46] Lupo, C., Ottaviani, C., Papanastasiou, P. & Pirandola, S. Continuous-variable measurement-device-independent quantum key distribution: Composable security against coherent attacks. *Phys. Rev. A* **97**, 052327 (2018).
- [47] Wu, Y. *et al.* Continuous-variable measurement-device-independent multipartite quantum communication. *Phys. Rev. A* **93**, 022325 (2016).
- [48] Vedral, V. The role of relative entropy in quantum information theory. *Rev. Mod. Phys.* **74**, 197–234 (2002).
- [49] Vedral, V., Plenio, M. B., Rippin, M. A. & Knight, P. L. Quantifying entanglement. *Phys. Rev. Lett.* **78**, 2275–2279 (1997).
- [50] Vedral, V. & Plenio, M. B. Entanglement measures and purification procedures. *Phys. Rev. A* **57**, 1619–1633 (1998).



- [51] Banchi, L., Braunstein, S. L. & Pirandola, S. Quantum fidelity for arbitrary Gaussian states. *Phys. Rev. Lett.* **115**, 260501 (2015).
- [52] Giorda, P. & Paris, M. G. A. Gaussian quantum discord. *Phys. Rev. Lett.* **105**, 020503 (2010).
- [53] Adesso, G. & Datta, A. Quantum versus classical correlations in Gaussian states. *Phys. Rev. Lett.* **105**, 030501 (2010).
- [54] Pirandola, S., Spedalieri, G., Braunstein, S. L., Cerf, N. & Lloyd, S. Optimality of Gaussian discord. *Phys. Rev. Lett.* **113**, 140405 (2014).
- [55] Pirandola, S. Quantum discord as a resource for quantum cryptography. *Sci. Rep.* **4**, 6956 (2014).
- [56] Eisert, J., Scheel, S. & Plenio, M. B. Distilling Gaussian states with Gaussian operations is impossible. *Phys. Rev. Lett.* **89**, 137903 (2002).
- [57] Fiurásek, J. Gaussian transformations and distillation of entangled gaussian states. *Phys. Rev. Lett.* **89**, 137904 (2002).
- [58] Spedalieri, G., Ottaviani, C. & Pirandola, S. Covariance matrices under Bell-like detections. *Open Syst. Inf. Dyn.* **20**, 1350011 (2013).
- [59] Garcia-Patron, R. & Cerf, N. J. Unconditional optimality of Gaussian attacks against continuous-variable quantum key distribution. *Phys. Rev. Lett.* **97**, 190503 (2006).
- [60] Navascues, M., Grosshans, F. & Acin, A. Optimality of Gaussian attacks in continuous-variable quantum cryptography. *Phys. Rev. Lett.* **97**, 190502 (2006).
- [61] Pirandola, S., Braunstein, S. L. & Lloyd, S. Characterization of collective Gaussian attacks and security of coherent-state quantum cryptography. *Phys. Rev. Lett.* **101**, 200504 (2008).
- [62] Lin, D., Huang, D., Huang, P., Peng, J., & Zeng, G., High performance reconciliation for continuous variable quantum key distribution with LDPC code. *Int. J. Quant. Inf.* **13**, 1550010 (2015).
- [63] Milicevic, M., Feng, C., Zhang, Lei M., & Gulak, P.G., Quasi-cyclic multi-edge LDPC codes for long-distance quantum cryptography. *npj Quantum Information* **4**, 21 (2017).
- [64] Lupo, C., Ottaviani, C., Papanastasiou, P. & Pirandola, S. Parameter estimation with almost no public communication for continuous-variable quantum key distribution. *Phys. Rev. Lett.* **120**, 220505 (2018).
- [65] Ruppert, L., Usenko, V. C. & Filip, R. Long-distance continuous-variable quantum key distribution with efficient channel estimation. *Phys. Rev. A* **90**, 062310 (2014).
- [66] Thearle, O., Assad, S. M., & Symul, T. Estimation of output-channel noise for continuous-variable quantum key distribution. *Phys. Rev. A* **93**, 042343 (2016).
- [67] Wang, C. *et al.* 25 MHz clock continuous-variable quantum key distribution system over 50 km fiber channel. *Sci. Rep.* **5**, 14607 (2015).
- [68] Pirandola, S. End-to-end capacities of a quantum communication network. *Comm. Phys.*, **2**, 51 (2019).
- [69] Pirandola, S. Capacities of repeater-assisted quantum communications. Preprint at <https://arxiv.org/abs/1601.00966> (2016).
- [70] Azuma, K., Mizutani, A., & Lo, H.K., Fundamental rate-loss trade-off for the quantum internet. *Nature Comm.*, **7**, 13523 (2016).
- [71] Rigovacca, L. *et al.* Versatile relative entropy bounds for quantum networks. *New J. Phys.* **20**, 013033 (2018).
- [72] Usenko, V. C., Ruppert, L., & Filip, R. Entanglement-based continuous-variable quantum key distribution with multimode states and detectors. *Phys. Rev. A* **90**, 062326 (2014).
- [73] Weinfurter, H. Experimental Bell-State Analysis. *Europhys. Lett.* **25**, 559 (1994).
- [74] Braunstein, S. L. & Mann, A. Measurement of the Bell operator and quantum teleportation. *Phys. Rev. A* **51**, R1727 (1995).
- [75] Pan, J.-W. & Zeilinger, A. Greenberger-Horne-Zeilinger-state analyzer. *Phys. Rev. A* **57**, 2208 (1998).
- [76] Qian, J., Feng, X. L. & Gong, S. Q. Universal Greenberger-Horne-Zeilinger-state analyzer based on two-photon polarization parity detection. *Phys. Rev. A* **72**, 052308 (2005).
- [77] Song, S., Cao, Y., Sheng, Y.-B. & Long, G.-L. Complete Greenberger-Horne-Zeilinger-state analyzer using hyperentanglement. *Quantum Inf. Process* **12**, 381 (2013).
- [78] Serikawa, T. & Furusawa, A. 500 MHz resonant photodetector for high-quantum-efficiency, low-noise homodyne measurement. *Rev. Sci. Instrum.* **89**, 063120 (2018).

# Supplementary Notes

## I. SUPPLEMENTARY NOTE 1: NETWORK IN THE ENTANGLEMENT-BASED REPRESENTATION

We study the security of our multipartite protocol adopting the entanglement-based (EB) representation, described in Supplementary Figure. S1. Each Bob prepares a two-mode squeezed vacuum state (TMSV)  $\Phi_{AB}$  where mode  $B$  is

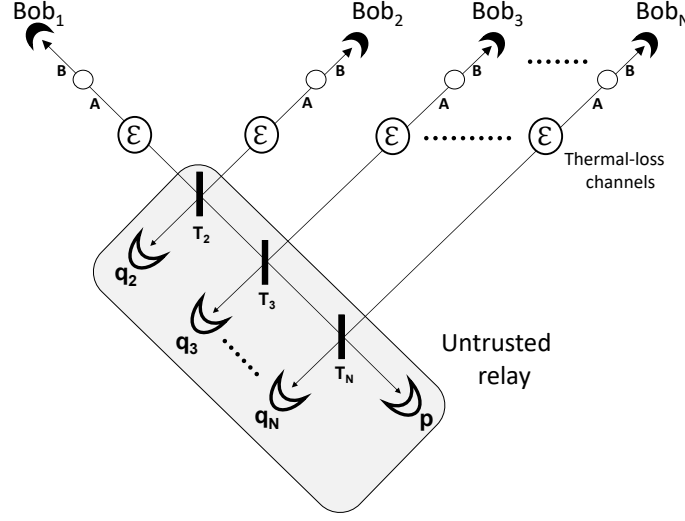


FIG. S1: Each Bob prepares a two-mode squeezed vacuum (TMSV) state  $\Phi_{AB}$ , composed by local mode  $B$  and the traveling mode  $A$ . The former is kept and measured, while the latter is sent through the communication channel to the untrusted relay, where the multipartite Bell detection is performed. In the squeezed protocol, conditional local squeezings are applied before Bobs' heterodynes.

kept while mode  $A$  is sent to the relay. Using the EB representation we may then consider two setups of the network.

- In a coherent-state configuration of the protocol, each Bob applies heterodyne detection on his local mode  $B$ , effectively projecting the traveling mode  $A$  into a Gaussian-modulated coherent state. This is the practical protocol presented in our main text, which can be easily done in prepare and measure.
- In a squeezed configuration of the protocol, the heterodyne detection on  $B$  is performed after the application of a local squeezing, so that a displaced squeezed state is remotely generated on mode  $A$ . Because the optimal local squeezing depends on the multipartite state shared by the Bobs after the Bell detection, this version of the protocol needs to be performed in the EB representation.

In the following Notes, we start by describing the mathematics of the multipartite Bell detection. Then, we consider the coherent-state protocol and the squeezed-state protocol. Both of them are studied from the point of view of quantum conferencing.

## II. SUPPLEMENTARY NOTE 2: MULTIPARTITE BELL DETECTION

In the main text we introduce a multipartite Bell measurement where  $N$  input modes first pass through an interferometer composed of  $N$  cascaded beam-splitters, and then are measured by homodyne detections with global outcome  $\gamma$ . In EB representation, the effect of the multipartite Bell detection is to distribute a conditional  $N$ -mode Gaussian state to the network users. Here we compute the covariance matrix (CM) of such  $N$ -mode conditional state. We start by showing a convenient dual representation for the multimode Bell detection, where the interferometer on  $A$  modes can be replaced by a conjugate one acting on the  $B$  modes. Then we compute the action of the homodyne detector on the  $A$  modes, and the symplectic transformation of the  $B$  modes.



### A. Dual representation of the multipartite Bell detection

Consider a system of  $N$  pairs of bosonic modes, where the quadrature vector of the  $k^{\text{th}}$  pair is denoted as

$$\xi_k = (\hat{q}_k^A, \hat{p}_k^A, \hat{q}_k^B, \hat{p}_k^B)^T, \quad (\text{S1})$$

for  $k = 1, \dots, N$  (this pair is in the hands of the  $k^{\text{th}}$  Bob). In a symmetric setting all the pairs of modes are prepared in the same state, which we assume to be a zero-mean Gaussian state with CM

$$\mathbf{V}_k = \begin{pmatrix} x & 0 & z & 0 \\ 0 & x & 0 & -z \\ z & 0 & y & 0 \\ 0 & -z & 0 & y \end{pmatrix}. \quad (\text{S2})$$

To represent the system of  $2N$  modes, we define the quadrature vector

$$\xi = (\xi^A, \xi^B)^T \quad (\text{S3})$$

$$= (\hat{q}_1^A, \hat{q}_2^A, \dots, \hat{q}_N^A, \hat{p}_1^A, \hat{p}_2^A, \dots, \hat{p}_N^A, \hat{q}_1^B, \hat{q}_2^B, \dots, \hat{q}_N^B, \hat{p}_1^B, \hat{p}_2^B, \dots, \hat{p}_N^B)^T, \quad (\text{S4})$$

so that the CM of the multimode state reads

$$\mathbf{V} = \begin{pmatrix} x\mathbf{I}_N & 0 & z\mathbf{I}_N & 0 \\ 0 & x\mathbf{I}_N & 0 & -z\mathbf{I}_N \\ z\mathbf{I}_N & 0 & y\mathbf{I}_N & 0 \\ 0 & -z\mathbf{I}_N & 0 & y\mathbf{I}_N \end{pmatrix}, \quad (\text{S5})$$

where  $\mathbf{I}_N$  is the  $N \times N$  identity matrix. Now we describe the action of the interferometer on this input state. The interferometer is described by a symplectic transformation on the  $A$  modes. Such a transformation maps the vector of  $A$  quadrature

$$\xi^A = (\hat{q}_1^A, \hat{q}_2^A, \dots, \hat{q}_N^A, \hat{p}_1^A, \hat{p}_2^A, \dots, \hat{p}_N^A)^T \quad (\text{S6})$$

as follows

$$\xi^A \rightarrow \begin{pmatrix} \mathbf{R} & 0 \\ 0 & \mathbf{R} \end{pmatrix} \xi^A, \quad (\text{S7})$$

where  $\mathbf{R}$  is a  $N \times N$  orthogonal matrix. This diagonal form follows from the fact that the beam-splitter transformations are chosen in such a way that they do not mix  $\hat{q}$ 's and  $\hat{p}$ 's. The transformation for the CM is

$$\mathbf{V} \rightarrow \mathbf{V}' = \begin{pmatrix} \mathbf{R} & 0 & 0 & 0 \\ 0 & \mathbf{R} & 0 & 0 \\ 0 & 0 & \mathbf{I}_N & 0 \\ 0 & 0 & 0 & \mathbf{I}_N \end{pmatrix} \begin{pmatrix} x\mathbf{I}_N & 0 & z\mathbf{I}_N & 0 \\ 0 & x\mathbf{I}_N & 0 & -z\mathbf{I}_N \\ z\mathbf{I}_N & 0 & y\mathbf{I}_N & 0 \\ 0 & -z\mathbf{I}_N & 0 & y\mathbf{I}_N \end{pmatrix} \begin{pmatrix} \mathbf{R}^T & 0 & 0 & 0 \\ 0 & \mathbf{R}^T & 0 & 0 \\ 0 & 0 & \mathbf{I}_N & 0 \\ 0 & 0 & 0 & \mathbf{I}_N \end{pmatrix}. \quad (\text{S8})$$

Applying  $\mathbf{R}^T \mathbf{R} = \mathbf{R} \mathbf{R}^T = \mathbf{I}_N$  to the specific form of the CM in Eq. (S5) we may write

$$\begin{aligned} \mathbf{V}' &= \begin{pmatrix} \mathbf{I}_N & 0 & 0 & 0 \\ 0 & \mathbf{I}_N & 0 & 0 \\ 0 & 0 & \mathbf{R}^T & 0 \\ 0 & 0 & 0 & \mathbf{R}^T \end{pmatrix} \begin{pmatrix} \mathbf{R} & 0 & 0 & 0 \\ 0 & \mathbf{R} & 0 & 0 \\ 0 & 0 & \mathbf{R} & 0 \\ 0 & 0 & 0 & \mathbf{R} \end{pmatrix} \begin{pmatrix} x\mathbf{I}_N & 0 & z\mathbf{I}_N & 0 \\ 0 & x\mathbf{I}_N & 0 & -z\mathbf{I}_N \\ z\mathbf{I}_N & 0 & y\mathbf{I}_N & 0 \\ 0 & -z\mathbf{I}_N & 0 & y\mathbf{I}_N \end{pmatrix} \begin{pmatrix} \mathbf{R}^T & 0 & 0 & 0 \\ 0 & \mathbf{R}^T & 0 & 0 \\ 0 & 0 & \mathbf{R}^T & 0 \\ 0 & 0 & 0 & \mathbf{R}^T \end{pmatrix} \begin{pmatrix} \mathbf{I}_N & 0 & 0 & 0 \\ 0 & \mathbf{I}_N & 0 & 0 \\ 0 & 0 & \mathbf{R} & 0 \\ 0 & 0 & 0 & \mathbf{R} \end{pmatrix} \\ &= \begin{pmatrix} \mathbf{I}_N & 0 & 0 & 0 \\ 0 & \mathbf{I}_N & 0 & 0 \\ 0 & 0 & \mathbf{R}^T & 0 \\ 0 & 0 & 0 & \mathbf{R}^T \end{pmatrix} \begin{pmatrix} x\mathbf{I}_N & 0 & z\mathbf{I}_N & 0 \\ 0 & x\mathbf{I}_N & 0 & -z\mathbf{I}_N \\ z\mathbf{I}_N & 0 & y\mathbf{I}_N & 0 \\ 0 & -z\mathbf{I}_N & 0 & y\mathbf{I}_N \end{pmatrix} \begin{pmatrix} \mathbf{I}_N & 0 & 0 & 0 \\ 0 & \mathbf{I}_N & 0 & 0 \\ 0 & 0 & \mathbf{R} & 0 \\ 0 & 0 & 0 & \mathbf{R} \end{pmatrix}. \end{aligned} \quad (\text{S9})$$

The meaning of this last equation is that the state obtained by passing the  $A$  modes through the interferometer described by the matrix  $\mathbf{R}$  is the same that would be obtained by passing the  $B$  modes through a conjugate interferometer described by the matrix  $\mathbf{R}^T$ . We have therefore found an equivalent dual representation for the multipartite Bell detection: Instead of first passing the  $A$  mode through the interferometer and then measure them, we can equivalently first measure the  $A$  modes and then pass the  $B$  modes through the conjugate interferometer. Of course this dual representation is valid as long as the total input CM takes the specific form in Eq. (S5).

### B. Homodyne detections

Let us assume the dual representation of the multipartite Bell detection. First we need to consider homodyne detection on the  $A$  modes. In our scheme only one mode (mode  $A_1$ ) is measured in the quadrature  $\hat{p}$ , while all the others are measured in the quadrature  $\hat{q}$ . Consider a pair of modes described by the CM in Eq. (S2). If the  $A$  mode is homodyned in the  $\hat{q}$  quadrature, the resulting conditional CM of the  $B$  mode is

$$\begin{pmatrix} y - z^2/x & 0 \\ 0 & y \end{pmatrix}. \quad (\text{S10})$$

If instead the  $\hat{p}$  quadrature is measured we obtain the conditional CM

$$\begin{pmatrix} y & 0 \\ 0 & y - z^2/x \end{pmatrix}. \quad (\text{S11})$$

Therefore, in terms of the vector of quadratures  $\xi^B = (\hat{q}_1^B, \hat{q}_2^B, \dots, \hat{q}_N^B, \hat{p}_1^B, \hat{p}_2^B, \dots, \hat{p}_N^B)^T$  the CM of the  $B$  modes, conditioned on the measurement output  $\gamma$  on the  $A$  modes, is

$$\mathbf{V}_{\mathbf{B}|\gamma}^{\text{in}} = \begin{pmatrix} \mathbf{V}_Q & 0 \\ 0 & \mathbf{V}_P \end{pmatrix}, \quad (\text{S12})$$

$$\mathbf{V}_Q := \begin{pmatrix} y & 0 \\ 0 & (y - z^2/x)\mathbf{I}_{N-1} \end{pmatrix}, \quad (\text{S13})$$

$$\mathbf{V}_P := \begin{pmatrix} y - z^2/x & 0 \\ 0 & y\mathbf{I}_{N-1} \end{pmatrix}. \quad (\text{S14})$$

This is the conditional CM of the  $B$  modes of the Bobs before the action of the conjugate interferometer (note that the Bobs know the first moments of their local reduced states from the value of the Bell outcome  $\gamma$ ).

### C. Action of the (conjugate) interferometer

The network of cascaded beam-splitters with transmissivities  $T_k = 1 - 1/k$ , for  $k = 1, \dots, N$ , as introduced in the main body of the paper, is described by the following linear transformations on the position quadratures

$$\hat{q}_1 \rightarrow \frac{1}{\sqrt{N}} \sum_{j=1}^N \hat{q}_j, \quad (\text{S15})$$

$$\hat{q}_k \rightarrow \sqrt{1 - k^{-1}} \left( \hat{q}_k - \frac{1}{k-1} \sum_{i=1}^{k-1} \hat{q}_i \right) \quad \text{for } k = 2, \dots, N, \quad (\text{S16})$$

together with analogous transformations on the momentum quadratures  $\hat{p}_j$ 's. We then obtain the elements of the symplectic matrix  $\mathbf{R}$

$$R_{1j} = \frac{1}{\sqrt{N}}, \quad (\text{S17})$$

$$R_{kj} = -\frac{1}{\sqrt{k(k-1)}} \quad \text{for } k = 2, \dots, N-1, \quad (\text{S18})$$

$$R_{kk} = \sqrt{1 - k^{-1}}. \quad (\text{S19})$$

From the interferometer  $\mathbf{R}$  we derive the conjugate interferometer  $\mathbf{R}^T$  and we compute the CM of the  $B$  modes from  $\mathbf{V}_{\mathbf{B}|\gamma}^{\text{in}}$ , finding

$$\mathbf{V}_{\mathbf{B}|\gamma} := \begin{pmatrix} \mathbf{V}'_Q & 0 \\ 0 & \mathbf{V}'_P \end{pmatrix} = \begin{pmatrix} \mathbf{R}^T \mathbf{V}_Q \mathbf{R} & 0 \\ 0 & \mathbf{R}^T \mathbf{V}_P \mathbf{R} \end{pmatrix}. \quad (\text{S20})$$

After simple algebra we find the following elements (for  $i, j = 1, \dots, N$ )

$$(\mathbf{V}'_Q)_{ij} = \sum_{k,l} R_{ki} V_{Qkl} R_{lj} \quad (\text{S21})$$

$$= y R_{1i} R_{1j} + \left(y - \frac{z^2}{x}\right) \sum_{k=2}^N R_{ki} R_{kj} \quad (\text{S22})$$

$$= \frac{z^2}{x} R_{1i} R_{1j} + \left(y - \frac{z^2}{x}\right) \sum_{k=1}^N R_{ki} R_{kj} \quad (\text{S23})$$

$$= \frac{z^2}{Nx} + \left(y - \frac{z^2}{x}\right) \delta_{ij}, \quad (\text{S24})$$

and similarly

$$(\mathbf{V}'_P)_{ij} = \sum_{k,l} R_{ki} V_{Pkl} R_{lj} = -\frac{z^2}{Nx} + y \delta_{ij}. \quad (\text{S25})$$

Thus, we have computed the conditional CM of Bobs'  $B$  modes after the multipartite Bell measurement with outcome  $\gamma$ . The resulting state  $\rho_{\mathbf{B}|\gamma}$  is symmetric under permutation of the  $B$  modes, and the correlation between any pair of modes scales as  $1/N$ . In particular, we may re-write this CM as follows

$$\mathbf{V}_{\mathbf{B}|\gamma} = \begin{pmatrix} \Delta & \Gamma & \dots & \Gamma \\ \Gamma & \Delta & \ddots & \Gamma \\ \vdots & \ddots & \ddots & \vdots \\ \Gamma & \Gamma & \dots & \Delta \end{pmatrix}, \quad (\text{S26})$$

with

$$\Gamma = \begin{pmatrix} \frac{z^2}{Nx} & 0 \\ 0 & -\frac{z^2}{Nx} \end{pmatrix}, \quad (\text{S27})$$

and

$$\Delta = \begin{pmatrix} y - \frac{N-1}{N} \frac{z^2}{x} & 0 \\ 0 & y - \frac{z^2}{Nx} \end{pmatrix}. \quad (\text{S28})$$

Now consider the  $i^{\text{th}}$  and  $j^{\text{th}}$  Bobs with quadrature vector  $\xi_{ij} = (\hat{q}_i^B, \hat{p}_i^B, \hat{q}_j^B, \hat{p}_j^B)^T$ . It is easy to check that the conditional (reduced) CM reads

$$\begin{aligned} \mathbf{V}_{B_i B_j|\gamma} &= \begin{pmatrix} \Delta & \Gamma \\ \Gamma & \Delta \end{pmatrix} \\ &= \begin{pmatrix} y - \frac{N-1}{N} \frac{z^2}{x} & 0 & \frac{z^2}{Nx} & 0 \\ 0 & y - \frac{z^2}{Nx} & 0 & -\frac{z^2}{Nx} \\ \frac{z^2}{Nx} & 0 & y - \frac{N-1}{N} \frac{z^2}{x} & 0 \\ 0 & -\frac{z^2}{Nx} & 0 & y - \frac{z^2}{Nx} \end{pmatrix}. \end{aligned} \quad (\text{S29})$$

### III. SUPPLEMENTARY NOTE 3: COHERENT-STATE PROTOCOL

#### A. Holevo bound

In order to compute Eve's Holevo information we exploit the fact that  $\rho_{\mathbf{E}|\gamma}$  is pure, where  $\mathbf{E}$  are Eve's output modes. We also use the fact that, after the heterodyne of the  $i^{\text{th}}$  Bob with outcome  $\beta_i$ , the conditional state  $\rho_{\mathbf{E}|\gamma\beta_i}$  with  $\mathbf{B}_i := B_1, \dots, B_{i-1}, B_{i+1}, \dots, B_N$  is pure. Therefore, we may write the Holevo bound as

$$\chi(\beta_i : \mathbf{E}) = S(\rho_{\mathbf{E}|\gamma}) - S(\rho_{\mathbf{E}|\gamma\beta_i}) = S(\rho_{\mathbf{B}|\gamma}) - S(\rho_{\mathbf{B}_i|\gamma\beta_i}), \quad (\text{S30})$$

where  $S$  is the von Neumann entropy. These entropic terms can therefore be computed from Bobs' CM  $V_{\mathbf{B}|\gamma}$  of Eq. (S26). This has a single  $N$ -degenerate symplectic eigenvalues, given by the following expression

$$\nu = \sqrt{y \left( y - \frac{z^2}{x} \right)}, \quad (\text{S31})$$

where we defined

$$x := \eta\mu + (1 - \eta)\omega, \quad y := \mu, \quad z := \sqrt{\eta(\mu^2 - 1)}. \quad (\text{S32})$$

From Eq. (S31) we obtain the total von Neumann entropy, given by

$$S(\rho_{\mathbf{B}|\gamma}) = Nh(\nu), \quad (\text{S33})$$

where

$$h(x) := \frac{x+1}{2} \log \frac{x+1}{2} - \frac{x-1}{2} \log \frac{x-1}{2}. \quad (\text{S34})$$

Then we compute the symplectic spectrum of the conditional CM  $V_{\mathbf{B}_i|\gamma\beta_i}$ . This corresponds to state  $\rho_{\mathbf{B}_i|\gamma\beta_i}$ , which describes the state of the  $N-1$  users conditioned to heterodyne detection on one arbitrary Bob. The doubly conditional CM is  $\mathbf{V}_{\mathbf{B}_i|\gamma\beta_i}$ , and has  $N-2$  identical symplectic eigenvalues given by Eq. (S31), and one given by the following expression

$$\nu_N = \sqrt{\frac{\lambda\bar{\lambda}}{\tau\bar{\tau}}}, \quad (\text{S35})$$

where

$$\lambda := N\omega\mu + \eta[1 + (N-1-N\omega)\mu], \quad (\text{S36})$$

$$\bar{\lambda} := N\omega\mu + \eta[N-1 - (N\omega-1)\mu], \quad (\text{S37})$$

$$\tau := N\omega(1-\eta) + \eta(N-1+\mu), \quad (\text{S38})$$

$$\bar{\tau} := N\omega(1-\eta) + \eta[(N-1)\mu+1]. \quad (\text{S39})$$

Then we may compute the following conditional von Neumann entropy

$$S(\rho_{\mathbf{B}_i|\gamma\beta_i}) = (N-2)h(\nu) + h(\nu_N), \quad (\text{S40})$$

which, together with Eq. (S33), gives the following Holevo bound

$$\chi(\beta_i : \mathbf{E}) = 2h(\nu) - h(\nu_N). \quad (\text{S41})$$

## B. Mutual information

The state of two given users is described by the CM of Eq. (S29). To compute the mutual information between two Bob, we need the conditional CM after local heterodyne measurement, i.e., we may apply the formula for heterodyne detection to CM  $\mathbf{V}_{B_i B_j|\gamma}$ , obtaining

$$\mathbf{V}_{B_i|\gamma\beta_j} = \mathbf{\Delta} - \mathbf{\Gamma}[\mathbf{\Delta} + \mathbf{I}]^{-1}\mathbf{\Gamma}, \quad (\text{S42})$$

from which it is simple to compute the mutual information between the two users, which is given by

$$I(\beta_i : \beta_j) = \frac{1}{2} \log_2 \frac{\sigma_s}{\sigma_n}, \quad (\text{S43})$$

with

$$\begin{aligned} \sigma_s &= 1 + \det \mathbf{V}_{B_i|\gamma} + \text{Tr} \mathbf{V}_{B_i|\gamma}, \\ \sigma_n &= 1 + \det \mathbf{V}_{B_j|\gamma\beta_i} + \text{Tr} \mathbf{V}_{B_j|\gamma\beta_i}. \end{aligned} \quad (\text{S44})$$

It is interesting to study the behavior of  $I(\beta_i : \beta_j)$  in terms of the number of users  $N$  and the Gaussian modulation  $\mu$ . We can check that, for  $N = 2$  and large modulation ( $\mu \gg 1$ ), one has

$$\sigma_n^{N=2} = \frac{4[\omega(1-\eta) + \eta]^2}{\eta^2}, \quad (\text{S45})$$

which recovers the result of Ref. [43] for standard CV-MDI-QKD. More generally, for  $N > 2$ , we find

$$\sigma_n^{N>2} = \frac{2(N-2)[\omega(1-\eta) + \eta]}{(N-1)\eta} \mu + f(\eta, \omega, N), \quad (\text{S46})$$

where  $f(\eta, \omega, N)$  is a function that does not depend on the modulation  $\mu$ . Because  $\sigma_n^{N>2}$  has a linear dependence in  $\mu$ , the key rate and the achievable distance decrease for increasing  $\mu$ . This means that an optimal  $\mu$  needs to be identified in terms of the other parameters. We implicitly assume this optimization in the computation of the key rate

$$K = I(\beta_i : \beta_j) - \chi(\beta_i : \mathbf{E}). \quad (\text{S47})$$

#### IV. SUPPLEMENTARY NOTE 4: SQUEEZED PROTOCOL

##### A. Local squeezing

Better key rates in terms of bits per use are obtained if the users apply local active operations, namely squeezing, before their heterodyne detections. Let us consider the reduced CM  $\mathbf{V}_{B_i B_j | \gamma} = \mathbf{V}_{B_i B_j | \gamma}(x, y, z, N)$  in Eq. (S29), and define the following parameters

$$s := \sqrt{\frac{y - \kappa}{y - \kappa(N-1)}}, \quad \kappa := \frac{z^2}{Nx}. \quad (\text{S48})$$

The local squeezing operations are chosen in such a way to transform  $\mathbf{V}_{B_i B_j | \gamma}$  into

$$\mathbf{W}_{B_i B_j | \gamma} = \begin{pmatrix} \alpha & \epsilon \\ \epsilon & \alpha \end{pmatrix}, \quad (\text{S49})$$

where

$$\alpha = \sqrt{(y - \kappa)[y - \kappa(N-1)]} \mathbf{I}, \quad \epsilon = \kappa \text{diag}(s, s^{-1}) \mathbf{Z}, \quad (\text{S50})$$

with  $\mathbf{I} = \text{diag}(1, 1)$  and  $\mathbf{Z} = \text{diag}(1, -1)$ . Assuming that all Bobs perform such local operations, the total conditional CM  $\mathbf{W}_{\mathbf{B} | \gamma}$  becomes

$$\mathbf{W}_{\mathbf{B} | \gamma} = \begin{pmatrix} \alpha & \epsilon & \cdots & \epsilon \\ \epsilon & \alpha & \ddots & \epsilon \\ \vdots & \ddots & \ddots & \vdots \\ \epsilon & \epsilon & \cdots & \alpha \end{pmatrix}. \quad (\text{S51})$$

Now assume the propagation of the  $A$  modes through thermal-loss channels with equal transmissivity  $\eta$  and equal thermal variance  $\omega = 2\bar{n} + 1$  with  $\bar{n}$  the mean number of photons. Then, we may write  $x = \eta\mu + (1-\eta)\omega$ ,  $y = \mu$ ,  $z = \sqrt{\eta(\mu^2 - 1)}$  and therefore

$$\kappa = \frac{\eta(\mu^2 - 1)}{N[\eta\mu + (1-\eta)\omega]}. \quad (\text{S52})$$

It is clear that the local squeezings are conditional, i.e., they are fully determined once the CM  $\mathbf{V}_{B_i B_j | \gamma}$  is known to the Bobs. This means that they need to retain their local modes  $B$  until after parameter estimation. Once the CM is known they may then apply their local operations. Also note that these operations cannot be simulated in the classical post-processing because they are not passive but active (squeezing). For this reason this version of the protocol can only be performed in EB representation and not in prepare and measure.

### B. Holevo bound

For the computation of the Holevo function, the only change occurs on the conditional von Neumann entropy. We then compute the symplectic spectrum of the CM  $\mathbf{W}_{\mathbf{B}_i|\gamma\beta_i}$  of the state  $\tilde{\rho}_{\mathbf{B}_i|\gamma\beta_i}$ . We find the previous symplectic eigenvalue  $\nu$  of Eq. (S31) with  $N - 2$  multiplicity, and the eigenvalue

$$\tilde{\nu}_N = \frac{\mu(\mu - N\kappa) + \sqrt{(\mu - \kappa)(\mu - (N - 1)\kappa)}}{1 + \sqrt{(\mu - \kappa)(\mu - (N - 1)\kappa)}}. \quad (\text{S53})$$

Therefore, we may write

$$S(\tilde{\rho}_{\mathbf{B}_i|\gamma\beta_i}) = (N - 2)h(\nu) + h(\tilde{\nu}_N), \quad (\text{S54})$$

and we derive

$$\chi(\beta_i : \mathbf{E}) = 2h(\nu) - h(\tilde{\nu}_N). \quad (\text{S55})$$

As expected this result does not depend on  $i$ .

### C. Mutual information

The mutual information is computed using the CM  $\mathbf{W}_{B_i B_j|\gamma}$  in Eq. (S49). Heterodyning mode  $B_i$ , we derive

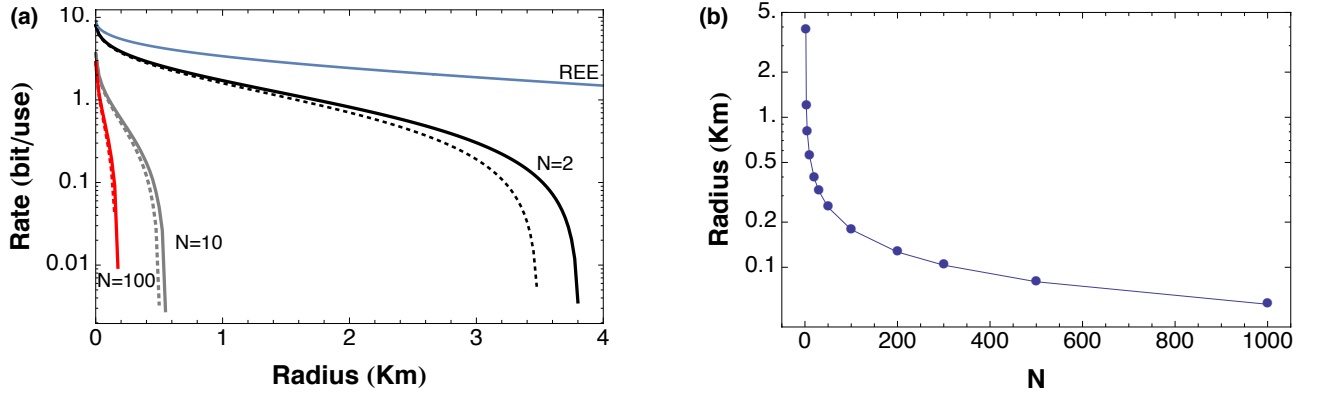


FIG. S2: Performance of the squeezed protocol, which is performed in the entanglement-based (EB) representation, where the various Bobs perform conditional local squeezings on their  $B$ -modes before detection. We plot the key rates and the maximum distances for quantum conferencing in panels (a) and (b). In (a) we plot the conferencing key rate for  $N = 2$  (black), 10 (grey) and 100 (red) users, as a function of the fiber distance  $d$  from the relay. We assumed an attenuation of 0.2dB/Km, and thermal noise  $\bar{n} = 0$  (solid curves) and  $\bar{n} = 0.05$  (dashed curves). The top blue curve is the upper bound provided by the relative entropy of entanglement (REE) of the reduced bipartite state specified by Eq. (S29). In panel (b) we plot the maximum fiber distance  $d$  from the relay versus the number of users  $N$ . From panel (a), we see that the use of squeezed states allows to improve the performance. The scheme allows to achieve a key rate of 0.1 per use for 100 users over a radius of 200m.

$$\mathbf{W}_{B_j|\gamma\beta_i} = \boldsymbol{\alpha} - \boldsymbol{\epsilon} [\boldsymbol{\alpha} + \mathbf{I}]^{-1} \boldsymbol{\epsilon}. \quad (\text{S56})$$

Therefore, we may compute the mutual information as [41]

$$I(\beta_i : \beta_j) = \frac{1}{2} \log_2 \frac{\sigma_s}{\sigma_n}, \quad (\text{S57})$$

where

$$\begin{aligned} \sigma_s &= 1 + \det \mathbf{W}_{B_i|\gamma} + \text{Tr} \mathbf{W}_{B_i|\gamma}, \\ \sigma_n &= 1 + \det \mathbf{W}_{B_j|\gamma\beta_i} + \text{Tr} \mathbf{W}_{B_j|\gamma\beta_i}. \end{aligned} \quad (\text{S58})$$

As previously mentioned, the optimal  $\mu$  needs to be identified in terms of the other parameters, and then used to compute the key rate

$$K = I(\beta_i : \beta_j) - \chi(\beta_i : \mathbf{E}) . \quad (\text{S59})$$

The optimal performance of quantum conferencing in this type of protocol is shown in Supplementary Figure S2(a,b). From Supplementary Figure S2(a), we see that 100 Bobs within a radius of 200m from the relay may extract a key rate at about 0.1 bits per use.

## V. SUPPLEMENTARY NOTE 5: MDI-QKD STAR NETWORK WITH DISCRETE-VARIABLE SYSTEMS

Let us now discuss a discrete-variable version of the MDI-QKD star network. In particular, we here show that linear optical implementations of this network lead to arbitrarily small rates as the number  $N$  of remote users increases, no matter how distant these users are. In particular, we provide two basic designs which have two different types of detection at the untrusted relay, with different costs in terms of bits of CCs. In the entanglement-based representation, suppose that each of the  $N$  Bobs has a Bell pair  $\Phi_{AB} := |\Phi\rangle_{AB} \langle\Phi|$  with  $|\Phi\rangle := (|00\rangle + |11\rangle)/\sqrt{2}$ . Bob keeps the  $B$ -qubit while sending the  $A$ -qubit to the untrusted relay (since we are interested in an upper bound, we assume there is no loss and noise in the links, which are therefore identity channels). Then, the relay detects all the received  $A$ -qubits in order to generate an  $N$ -qubit GHZ state  $|\text{GHZ}_N^+\rangle := (|00\dots 0\rangle + |11\dots 1\rangle)/\sqrt{N}$  for the remote  $B$ -qubits.

### A. First design

In a first design, the relay prepares  $N$  local qubits  $C_1 \dots C_N$  in the state  $|\text{GHZ}_N^+\rangle$ . Then, each  $C_i$ -qubit is measured with a corresponding  $A_i$ -qubit in a standard qubit Bell detection, with 4 possible outcomes. After communicating 2 classical bits to the  $i$ th Bob, the latter can implement a local Pauli correction, so that the state of the  $C_i$ -qubit is perfectly teleported to the remote  $B_i$ -qubit. Globally, the  $N$  Bell detections and the  $2N$  bits of CC allow one to swap  $|\text{GHZ}_N^+\rangle$  in the remote  $B$ -qubits. The problem appears when we want to implement this scheme practically with linear optics. In fact, any linear optical realization of a qubit Bell detection has 1/2 probability of success [37, 73, 74]. The probability of having  $N$  successful Bell detections, and therefore swapping  $|\text{GHZ}_N^+\rangle$ , is therefore  $p_{\text{succ}} = 2^{-N}$ . Clearly this prevents to share an  $N$ -partite conference key for large  $N$ , no matter at what distance the Bobs are.

### B. Second design

We may consider a different joint measurement at the untrusted relay. Given  $|\text{GHZ}_N^+\rangle$  and  $|\text{GHZ}_N^-\rangle := (|00\dots 0\rangle + |11\dots 1\rangle)/\sqrt{N}$ , one may construct a basis of  $2^N$  orthonormal states by applying the identity  $I$  and bit-flip Pauli operators  $X$  to  $|\text{GHZ}_N^\pm\rangle$ . For instance, for  $N = 3$ , we may build the 8 states (up to normalization)

$$I \otimes I \otimes I |\text{GHZ}_3^\pm\rangle = |000\rangle \pm |111\rangle, \quad (\text{S60})$$

$$I \otimes I \otimes X |\text{GHZ}_3^\pm\rangle = |001\rangle \pm |110\rangle, \quad (\text{S61})$$

$$I \otimes X \otimes I |\text{GHZ}_3^\pm\rangle = |010\rangle \pm |101\rangle, \quad (\text{S62})$$

$$X \otimes I \otimes I |\text{GHZ}_3^\pm\rangle = |100\rangle \pm |011\rangle. \quad (\text{S63})$$

For  $N = 4$ , we may build the  $2^4 = 16$  states

$$I \otimes I \otimes I \otimes I |\text{GHZ}_4^\pm\rangle = |0000\rangle \pm |1111\rangle, \quad (\text{S64})$$

$$I \otimes I \otimes I \otimes X |\text{GHZ}_4^\pm\rangle = |0001\rangle \pm |1110\rangle \quad (\text{S65})$$

$$I \otimes I \otimes X \otimes I |\text{GHZ}_4^\pm\rangle = |0010\rangle \pm |1101\rangle, \quad (\text{S66})$$

$$I \otimes X \otimes I \otimes I |\text{GHZ}_4^\pm\rangle = |0100\rangle \pm |1011\rangle, \quad (\text{S67})$$

$$X \otimes I \otimes I \otimes I |\text{GHZ}_4^\pm\rangle = |1000\rangle \pm |0111\rangle, \quad (\text{S68})$$

$$I \otimes I \otimes X \otimes X |\text{GHZ}_4^\pm\rangle = |0011\rangle \pm |1100\rangle, \quad (\text{S69})$$

$$I \otimes X \otimes I \otimes X |\text{GHZ}_4^\pm\rangle = |0101\rangle \pm |1010\rangle, \quad (\text{S70})$$

$$X \otimes I \otimes I \otimes X |\text{GHZ}_4^\pm\rangle = |1001\rangle \pm |0110\rangle. \quad (\text{S71})$$



For generic  $N \geq 3$ , the  $2^N$  basis states are built by considering all the various combinations in which we can apply the bit-flip operators. The orthogonal projectors onto this basis  $\{\Pi_1, \dots, \Pi_k, \dots, \Pi_{2^N}\}$  provide a von Neumann measurement. After the relay performs this measurement on all the  $A$ -qubits, it broadcasts the  $N$  classical bits of the outcome  $k$  to all Bobs. The latter may therefore apply  $X$  or  $I$  operators on their  $B$ -qubits so that they share the state  $|\text{GHZ}_N^\pm\rangle$ , which can always be transformed into  $|\text{GHZ}_N^+\rangle$  by means of a single phase-flip Pauli operator  $Z$ . Again the problem appears when we want to implement this scheme practically with linear optics. In fact, as shown in Ref. [75], a GHZ-state analyzer based on linear optics can only distinguish two among  $2^N$  maximally-entangled GHZ states. This means that the probability of success is equal to  $p_{\text{succ}} = 2^{1-N}$ . It is clear that the use of non-linearities may improve this performance [76], but the scheme rapidly becomes highly impractical for increasing  $N$ . Similarly, there is no room for improving the performance by resorting to hyper-entanglement [77], just because the protocol is strictly based on a single degree of freedom (e.g., polarization).

## VI. SUPPLEMENTARY NOTE 6: STUDY OF IMPERFECTIONS FOR A PROOF-OF-PRINCIPLE EXPERIMENT

Here we study the impact of practical imperfections on the performance of our scheme, i.e., on the key rate and achievable distance within each module  $M_i$ . The degradation of performances are caused by optical losses that, for instance, may arise from anti-reflection coating of the beam splitters, and imperfect beam interferences. Optical losses impact on the performance mainly because they degrade the operation realized by the relay. These are analyzed including non-ideal efficiencies of the relays' detectors (Case 1), and we also consider the combined effect of detection efficiency and imperfect beam interference (Case 2).

### A. Case 1

Optical losses are simulated by placing  $N$  identical beam splitters with transmissivity  $\tilde{\eta}$  before the homodyne detections realized by the relay. It is important to stress that the presence of the detector efficiencies  $\tilde{\eta}$  preserves the

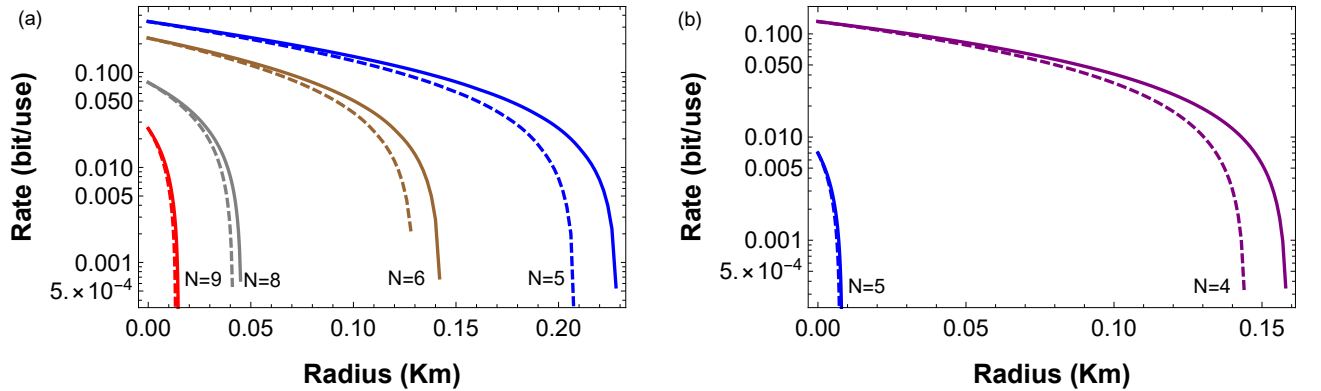


FIG. S3: This figure shows the optimal key-rate versus the achievable distance. In panel (a) we plot the key rates for detector efficiency  $\tilde{\eta} = 99\%$ , considering  $N = 5$  (blue), 6 (brown), 8 (gray), 9 (red) users, pure-loss attacks ( $\omega = 1$ , solid), and thermal-loss attacks with  $n_{th} = 0.05$  (dashed). The curves in panel (b) are obtained considering  $\tilde{\eta} = 98\%$ , for  $N = 4$  (purple) and 5 (blue).

symmetric structure of the CM in Eq. (S26) (see, for instance, the case with two-users discussed in ref. [43]). In such a case, the only change occurring is in the quantity  $x$  of Eq. (S32), which can be redefined as follows

$$\tilde{x} := \eta\mu + (1 - \eta)\omega + \frac{1 - \tilde{\eta}}{\tilde{\eta}}. \quad (\text{S72})$$

Keeping the symmetric structure of the CM (S26) allows us to obtain analytical results. In particular, it is simple to see that the  $N$ -fold degenerate total symplectic eigenvalue of Eq. (S31) acquires now the following expression

$$\tilde{\nu} = \sqrt{y \left( y - \frac{z^2}{\tilde{x}} \right)}, \quad (\text{S73})$$

while the conditional spectrum is given by  $\tilde{\nu}$ ,  $(N - 2)$ -fold degenerate, and by

$$\tilde{\nu}_N = \sqrt{\frac{[N\tilde{\omega}\mu + \eta(1 + (N - 1 - N\omega)\mu)][N\tilde{\omega}\mu + \eta[N - 1 - (N\omega - 1)\mu]]}{[N\tilde{\omega} + \eta(N - 1 + \mu - N\omega)][N\tilde{\omega} + \eta[1 + (N - 1)\mu - N\omega]]}}, \quad (\text{S74})$$

which is the same as the eigenvalue of Eq. (S35) with  $\tilde{\omega} := \omega + (1 - \tilde{\eta})/\tilde{\eta}$ . The eigenvalues of Eq. (S73) and (S74) are then used to compute the Holevo function  $\tilde{\chi}(\beta_i, \mathbf{E})$  using the formal expression of Eq. (S41) and replacing  $\nu \rightarrow \tilde{\nu}$  and  $\nu_N \rightarrow \tilde{\nu}_N$ . Similarly, the mutual information between two arbitrary Bobs is obtained from the two-mode CM  $\tilde{\mathbf{V}}_{B_i B_j}$ , having the same structure of CM  $\mathbf{V}_{B_i B_j}$  of Eq. (S29), replacing  $x \rightarrow \tilde{x}$ . Using the following definitions

$$a := y - \frac{N - 1}{N} \frac{z^2}{\tilde{x}}, \quad (\text{S75})$$

$$b := y - \frac{z^2}{N\tilde{x}}, \quad (\text{S76})$$

$$c := \frac{z^2}{N\tilde{x}}, \quad (\text{S77})$$

we write the general expression of the mutual information in the following compact form

$$\tilde{I}(\beta_i : \beta_j) = \frac{1}{2} \log_2 \frac{(a + 1)^2 (b + 1)^2}{[(1 + a)^2 - c^2][(1 + b)^2 - c^2]}, \quad (\text{S78})$$

and obtain the key rate

$$\tilde{K}_{ij}(\mu, \eta, \omega, N, \tilde{\eta}) := \tilde{I}(\beta_i : \beta_j) - \tilde{\chi}(\beta_i, \mathbf{E}). \quad (\text{S79})$$

The final key-rate, for fixed  $\eta, \omega, N$ , and  $\tilde{\eta}$ , is obtained by maximizing over modulation  $\mu$

$$\tilde{K}_{opt} = \max_{\mu} \tilde{K}_{ij}(\mu, \eta, \omega, N, \tilde{\eta}). \quad (\text{S80})$$

Using previous results, we studied the performance of a star network for several values of the number of users  $N$ . The presence of optical losses degrades the achievable distance, the key-rate and the number of users composing the star network. The results are described in Supplementary Figure S3, where we plot the optimal key rate considering pure-loss attacks ( $\omega = 1$ , solid lines), and symmetric thermal-loss attacks with mean thermal photon number  $\bar{n} = 0.05$  (dashed lines). In Supplementary Figure S3 (a) we show several key rates for increasing number of users, from right to left. We find that, for state-state-of-the-art detectors [78] with efficiency  $\tilde{\eta} = 0.99$ , a star network with  $N = 9$  components may generate secure keys within a radius of about 14 m. In Supplementary Figure S3 (b) we see the impact of slightly worse detectors ( $\tilde{\eta} = 0.98$ ). In such a case, for  $N = 5$  users, the achievable distance reduces to 8 m.

## B. Case 2

We consider now the additional optical losses caused by imperfect beam interference in the beam splitters  $T_k$  of the relay. In addition to the efficiency of the homodyne detectors, we then consider beam splitters with transmissivity defined as follows

$$T_k = 1 - \frac{1}{k} - \bar{\epsilon}, \text{ for } k = 2, \dots, N, \quad (\text{S81})$$

where the parameter  $\bar{\epsilon}$  describes the imperfect beam-splitter interference. We remark that the inclusion of parameter  $\bar{\epsilon}$  breaks the symmetry of the CM that does not have anymore the structure of Eq. (S26). In such a case, the key rate can be computed only numerically, and is defined as follows

$$\bar{K}_{opt} = \inf_{\{i,j\}} \left[ \max_{\mu} \tilde{K}_{ij}(\mu, \eta, \omega, N, \tilde{\eta}, \bar{\epsilon}) \right], \quad (\text{S82})$$

maximizing the key rates  $\tilde{K}_{ij}$  between two Bobs over the Gaussian modulation  $\mu$ , and taking the infimum over the pairs  $\{i, j\}$ . The results of this analysis are described in Supplementary Figure S4. The impact of parameter  $\bar{\epsilon}$  results in a further reduction of the achievable distance that, for  $\bar{\epsilon} = 1\%$  and  $N = 7$ , reduces to 12 m, while for  $N = 6$  it is

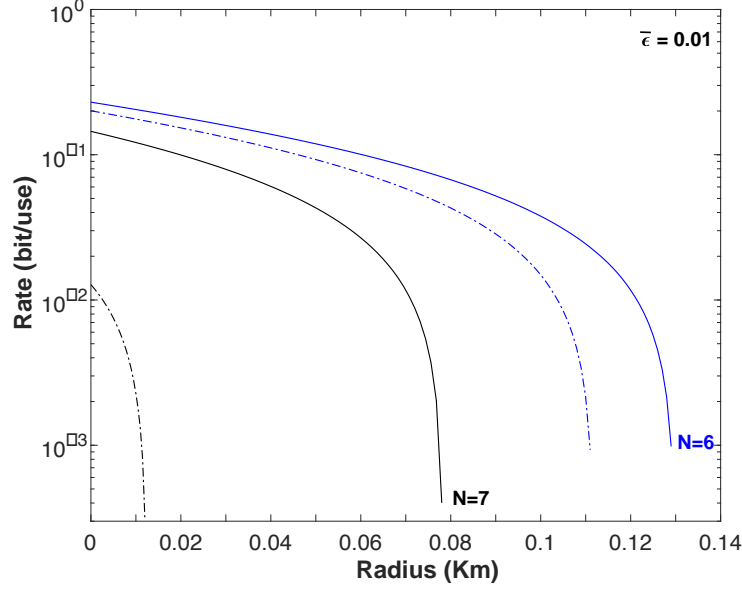


FIG. S4: This figure shows the optimal key-rate versus the achievable distance, to assess the combined effect of non-ideal detector efficiency  $\tilde{\eta} = 99\%$  and losses caused by imperfect beam interference (described by setting  $\bar{\epsilon} = 1\%$ ). We plot the optimal key rate of Eq. (S82) for  $N = 7$  (black), 6 (blue), assuming thermal-loss attacks with  $n_{th} = 0.05$  and  $\bar{\epsilon} = 0$  (solid lines) or 0.01 (dot-dashed). We find that the achievable distance for  $N = 7$  users reduces to about 12 m, while for  $N = 6$  the achievable distance from the relay is 111 m.

still 111m. We stress that, despite we find this degradation of the performance imposed by practical imperfections, larger number of users can be connected over arbitrary distances using the modular structure discussed in this work.

The key rates described in Supplementary Figures S3 and S4 are obtained from the asymptotic analysis and assuming an imperfect interferometer. Because our protocol is based on Gaussian modulation, the optimal attack is Gaussian and, without loss of generality, the CM formalism can be used to study the security performance. To determine the entries of the CM, one can use long data blocks ( $n \geq 10^7$ ) for the parameter estimation procedure, so as to achieve a precise estimation of attenuation and noise in the channels. In addition to this, the hybrid (classical/quantum) structure of our modular protocol avoids the degradation of the key in its propagation throughout the network, after the completion of quantum communication within each module.

Further analysis may be required to include the impact of additional imperfections which may play a role in a practical implementation of the scheme, especially for the case described in Supplementary Note 4. In such a case it may be necessary to consider the multimode structure of the sources and the local detectors, which may destabilize the achievable key rate and the security properties, as described in Ref. [72] for one-way protocols. However, the security properties of the single-mode analysis can be recovered by applying a suitable mode symmetrization that neutralizes the leakage of information towards the eavesdropper [72].